

# On Measuring Localization of Shortcuts in Deep Networks

Nikita Tsoy

INSAIT,

Sofia University “St. Kliment Ohridski”,  
Sofia, Bulgaria

Nikola Konstantinov

INSAIT,

Sofia University “St. Kliment Ohridski”,  
Sofia, Bulgaria

## Abstract

Shortcuts, spurious rules that perform well during training but fail to generalize, present a major challenge to the reliability of deep networks (Geirhos et al., 2020). However, the impact of shortcuts on feature representations remains understudied, obstructing the design of principled shortcut-mitigation methods. To overcome this limitation, we investigate the layer-wise localization of shortcuts in deep models. Our novel experiment design quantifies the layer-wise contribution to accuracy degradation caused by a shortcut-inducing skew by counterfactual training on clean and skewed datasets. We employ our design to study shortcuts on vision tasks: CIFAR-10, Waterbirds, and CelebA, across VGG, ResNet, DeiT, and ConvNeXt architectures. We find that shortcut learning is not localized in specific layers but distributed throughout the network. Different network parts play different roles in this process: shallow layers predominantly encode spurious features, while deeper layers predominantly forget core features that are predictive on clean data. We also analyze the differences in localization and describe its principal axes of variation. Finally, our analysis of layer-wise shortcut-mitigation strategies suggests the hardness of designing general methods, supporting dataset- and architecture-specific approaches instead.

## 1 INTRODUCTION

*Shortcuts*, spurious rules that hold within training distributions but fail to generalize to real-world scenarios, present a major challenge to the reliability of deep networks. Despite their significance, the mechanisms underlying shortcut learning remain poorly understood.

While shortcuts arise from a statistical phenomenon of spurious correlations (Arjovsky et al., 2020), it remains unclear how and which correlations are captured during training (Hermann and Lampinen, 2020).

A crucial yet underexplored dimension of shortcut learning is the hierarchical nature of deep networks. Since different layers correspond to distinct levels of abstraction and feature complexity (Simonyan et al., 2014), shortcuts likely manifest differently across layers. Quantifying the impact of this phenomenon on accuracy could inform the design of layer-specific interventions for shortcut mitigation (e.g., Lee et al., 2023). However, existing research falls short in this regard—either focusing solely on overall model accuracy without layer-specific effects (Scimeca et al., 2022) or analyzing feature representations without explicitly connecting these findings to test performance (Hermann and Lampinen, 2020; Islam et al., 2021).

**Contributions** To bridge this gap, we develop a method for quantifying the layer-wise effects of shortcuts on model accuracy. Our approach measures *each layer’s contribution to shortcut learning*, expressed as accuracy degradation on clean test data, by analyzing *counterfactual changes* in network behavior when trained on skewed and clean data. We decompose shortcut learning into two fundamental processes: spurious feature promotion and core feature degradation. And, we analyze them using two metrics: spurious feature encoding and core feature forgetting.

We apply our methodology in the context of vision models. In particular, we study a watermark skew on CIFAR-10, background skew on Waterbirds, and sampling skew on CelebA, across the VGG-11, ResNet-18, DeiT-Ti, and ConvNeXt-T architectures. Our findings reveal that shortcut learning is not localized in specific layers, but is instead distributed throughout the whole network. Different layers play different roles in shortcut learning: shallow layers mostly contribute to spurious feature encoding, while deep layers mostly contribute to core feature forgetting. Dataset and model

factors explain 87.0% of variance in encoding localization, while data skew frequency and optimizer factors explain 62.3% of variance in forgetting localization in fine-tuned models. Finally, we find that our metrics predict the success of some layer-wise interventions.

From a practical standpoint, localization varies a lot across different datasets and architectures. Additionally, our localization metrics predict the success of some layer-wise specific interventions (e.g., layer freezing). Together, these findings suggest that layer-wise vision shortcut mitigation strategies should be dataset- and architecture-specific.

## 2 RELATED WORK

**Impact of Shortcuts on Feature Representations** Several studies examine the impact of shortcuts on representations (Hermann and Lampinen, 2020; Islam et al., 2021; Scimeca et al., 2022). They analyze how shortcuts are encoded in layers through linear probing accuracy (Hermann and Lampinen, 2020), mutual information and read-out module accuracy (Islam et al., 2021), or validation accuracy on feature-labeled datasets (Scimeca et al., 2022). While these approaches provide valuable insights, they do not explicitly attribute accuracy degradation to specific layers. In contrast, our work directly quantifies *layer-wise contributions to accuracy degradation*, offering a more direct assessment of each layer’s role in shortcuts.

**Mechanisms of Shortcut Formation** Our work contributes to the literature on shortcut learning mechanisms (Shah et al., 2020; Sagawa et al., 2020; Nagarajan et al., 2021; Chaudhuri et al., 2023; Puli et al., 2023; Wang et al., 2023; Tsoy and Konstantinov, 2024). Our analysis suggests that feature forgetting plays a key role in shortcuts, supporting prior hypotheses that simplicity bias (e.g., Shah et al., 2020) or excessive regularization (Sagawa et al., 2020) are important for shortcut formation. In contrast to these works, we measure the contributions to shortcut learning by different parts of the network, allowing for a fine-grained quantitative understanding of shortcuts.

**Quantification of Layers’ Importance** Similarly to us, Zhang et al. (2022); Maini et al. (2023); Huh et al. (2023) investigate feature representations in deep models and assess the importance of each layer for specific model properties. Zhang et al. (2022) measure the importance of each layer of a deep network for classification accuracy by injecting noise in the network weights. Maini et al. (2023) analyze the memorization behavior of different layers by introducing label noise. Huh et al. (2023) analyze learned feature representations of deep models and show how some of their prop-

erties help generalization. While these studies provide valuable insights into feature learning, they do not study shortcut learning. Thus, these approaches are not directly comparable to our methodology.

**Layer-Wise Fine-Tuning Analysis** Our work is related to the literature on layer-wise adaptation of deep models to distribution shifts (e.g., Kumar et al., 2022; Lee et al., 2023; Trivedi et al., 2023; Kirichenko et al., 2023). Our findings help to reason about fine-tuning strategies for shortcut mitigation. We refer to our conclusion section for further discussion.

## 3 METHODOLOGY

This section outlines our method for measuring *layer-wise contributions* to shortcut learning. Our approach introduces controlled *shortcut-inducing skews* into the training process, such as replacing the background of an image with a class-correlated one, like in Waterbirds (Sagawa\* et al., 2020). This approach allows us to assess each layer’s role *counterfactually*, by controlling all factors of training except for the data itself. We train multiple networks on the same task, exposing different blocks of layers to skewed or clean (skew-free) data and evaluate these networks on a clean test dataset to quantify each block’s contribution.

### 3.1 Illustrative Example

We start with an architecture  $h = (c, f)$  consisting of a classifier  $c$  and feature extractor  $f$ :  $h(\cdot) = c(\cdot) \circ f(\cdot)$ . Consider training this architecture on two datasets: a clean  $D^c$  and a skewed  $D^s$  ones, resulting in two models  $h^c = (c^c, f^c)$  and  $h^s = (c^s, f^s)$ , respectively. Due to shortcut learning, we expect to see an increase in test error rate on clean data,  $\text{er}(h^s) - \text{er}(h^c)$ .

We aim to quantify the contributions of the classifier  $c$  and feature extractor  $f$  to the increase in test error rate  $\text{er}(h^s) - \text{er}(h^c)$ . Specifically, we are interested in how spurious (that emerge due to the skew) and core features (that are predictive on clean data) are encoded and used. Let  $c^{c,f^s}$  denote a classifier retrained on clean data using the skewed extractor  $f^s$  and  $c^{s,f^c}$  denote a classifier retrained on skewed data using the clean extractor  $f^c$  (see details in Section 3.3). We consider the following two decompositions:

$$\begin{aligned} & \text{er}(h^s) - \text{er}(h^c) \\ &= \text{er}(c^s, f^s) - \text{er}(c^{s,f^c}, f^c) + \text{er}(c^{s,f^c}, f^c) - \text{er}(c^c, f^c) \\ &= \text{er}(c^s, f^s) - \text{er}(c^{c,f^s}, f^s) + \text{er}(c^{c,f^s}, f^s) - \text{er}(c^c, f^c). \end{aligned} \tag{1}$$

We interpret the first decomposition in the following manner. In the term  $\text{er}(c^s, f^s) - \text{er}(c^{s,f^c}, f^c)$ , both classifiers are trained on the skewed data. Hence, this term

isolates the effect of the extractor on the propensity of the classifier to rely on spurious correlations. Thus, this term measures the increase in *spurious feature encoding* by the skewed feature extractor compared to the clean one. In the term  $\text{er}(\textcolor{red}{c^s, f^c}) - \text{er}(\textcolor{blue}{c^c, f^c})$ , both models use the same extractor. Hence, this term isolates the effect of training data on the reliance of the classifier on core features. Thus, this term measures the *core feature underutilization* caused by the skew in the retrained classifier.

Similarly,  $\text{er}(\textcolor{red}{c^s, f^s}) - \text{er}(\textcolor{blue}{c^c, f^s})$  measures *spurious feature amplification* in the skewed classifier and  $\text{er}(\textcolor{red}{c^c, f^s}) - \text{er}(\textcolor{blue}{c^c, f^c})$  corresponds to *core feature forgetting* by the skewed feature extractor.<sup>1</sup>

**Shortcut Learning Metrics** To measure how spurious and core features are localized and used, we use two metrics: *spurious feature encoding* and *core feature forgetting*. They determine how much the extractor “incentivizes” the classifier to rely on spurious features or “disincentives” the classifier to rely on clean features, respectively. In our work, we aim to localize blocks’ contributions to these phenomena to better understand the mechanisms of shortcut learning. Note also that the other metrics: *spurious feature amplification* and *core feature underutilization*, complement the chosen ones, making their localization symmetrical.

**Counterfactual Training Algorithm** A crucial aspect for objectively measuring these metrics is the design of an appropriate classifier retraining scheme. Retraining needs to maintain consistency between the learning mechanisms in the original and new classifier retraining, i.e., it should *control for all factors apart from the training data itself*, to avoid biases in localization measures. At the same time, due to over-parametrization (Brunet et al., 2022) and implicit biases (e.g., Nagarajan et al., 2021), deep learning is highly sensitive to even small changes in training procedure, making this task non-trivial.

### 3.2 Shortcut Learning Metrics

In the general case, we consider a feed-forward architecture consisting of  $m$  blocks of layers

$$f(\theta, \cdot) = f_{m-1}(\theta_{m-1}, \cdot) \circ f_{m-2}(\theta_{m-2}, \cdot) \circ \dots \circ f_0(\theta_0, \cdot). \quad (2)$$

Let  $\theta_A$  represent the weights of blocks  $i \in A$ , where  $A \subseteq [m]$  and  $[m] := \{0, \dots, m-1\}$ . Define  $i:j := \{i, \dots, j-1\}$ , and let  $\text{er}(\theta)$  be the error rate of this architecture with weights  $\theta$  on the clean test dataset.

<sup>1</sup>While we expect all considered differences to be positive, it is generally not guaranteed. For example, some layers might be responsible for filtering out a shortcut rule because it does not have perfect predictive power.

Consider two networks trained on clean and skewed data, resulting in weights  $\theta^c$  and  $\theta^s$ , respectively. We interpret the increase in error rate  $\text{er}(\theta^s) - \text{er}(\theta^c)$  as a measure of shortcut learning. Our goal is to measure the contributions of individual blocks to this increase.

We investigate what would happen if some intervention subset of blocks  $A$  of the clean (skewed) model were *counterfactually trained* on skewed (clean) data. Let  $\theta^{c,A}$  be a model that shares blocks  $[m] \setminus A$  with the clean model, but whose subset of blocks  $A$  was counterfactually trained on the skewed data (with  $\theta^{s,A}$  defined analogously). As previously, we get decompositions

$$\text{er}(\theta^s) - \text{er}(\theta^c) = \text{enc}_{[m] \setminus A} + \text{uut}_A = \text{amp}_A + \text{fgt}_{[m] \setminus A},$$

where  $\text{enc}_{[m] \setminus A} := \text{er}(\theta^s) - \text{er}(\theta^{c,A})$  is the contributions of blocks  $[m] \setminus A$  to *spurious features encoding*,  $\text{uut}_A := \text{er}(\theta^{c,A}) - \text{er}(\theta^c)$  is the contributions of blocks  $A$  to *core features underutilization*,  $\text{fgt}_{[m] \setminus A} := \text{er}(\theta^{s,A}) - \text{er}(\theta^c)$  is the contributions of blocks  $[m] \setminus A$  to *core features forgetting*, and  $\text{amp}_A := \text{er}(\theta^s) - \text{er}(\theta^{s,A})$  is the contributions of blocks  $A$  to *spurious features amplification*. We often consider *relative contributions* normalized with  $\text{er}(\theta^s) - \text{er}(\theta^c)$  to allow fair comparison across datasets and architectures (see Section 4 for details).

Again, we can see that shortcut learning encompasses two processes: one related to core feature degradation (expressed as core feature forgetting or underutilization) and one related to spurious feature promotion (expressed as spurious feature amplification or encoding). Our framework allows us to quantify how different network parts contribute to these processes. Specifically, we focus on the spurious feature encoding and core feature forgetting metrics, with results on the localization of the other metrics being symmetrical.

### 3.3 Counterfactual Training Algorithm

As previously argued, a key challenge in our approach is the design of a *counterfactual training* procedure that preserves learning mechanisms across all models. There are several critical factors: ensuring all corresponding blocks have *equal exposure to training data*, maintaining *consistent optimizer configurations and hyperparameters* (as some hyperparameters, such as learning rate, significantly impact features, Li et al., 2019; Lewkowycz et al., 2020), and allowing blocks to *progressively adapt* to intermediate features since progressive adaptation invokes different learning mechanisms compared to static post-training (Allen-Zhu and Li, 2019; Panigrahi et al., 2024; Abbe et al., 2022).

We solve this challenge through a simultaneous training procedure described in Algorithm 1 (for brevity, we only consider training  $\theta^{c,A}$  with stochastic gradient descent (SGD), but extensions to training  $\theta^{s,A}$  and

other optimizers are straightforward). Here, the loss of a network with weights  $\theta$  on a data batch  $B$  is denoted by  $L(\theta, B)$ . This procedure trains the anchor clean network  $\theta^c$  and counterfactually intervened network  $\theta^{c,A}$  in parallel. In each round, we sample a clean data batch  $B_t$  and skewed data batch  $B'_t = g(B_t)$  to update the models. Since blocks  $[m] \setminus A$  are shared, we essentially only update  $\theta_A^{c,A}$  using skewed data during the backward pass through the network  $\theta^{c,A}$ .

**Algorithm 1** Simultaneous training of networks

```

Initialize  $\theta_0^c$  — anchor network weights
Initialize  $\theta_0^{c,A} = \theta_0^c$  — intervened network weights
for  $t = 1$  to  $T$  do
    Sample clean  $B_t$  and skewed  $B'_t = g(B_t)$  batches
    Update  $\theta_t^{c,A} = \theta_{t-1}^{c,A} - \eta_t \nabla L(\theta_{t-1}^{c,A}, B'_t)$ 
    Update  $\theta_t^c = \theta_{t-1}^c - \eta_t \nabla L(\theta_{t-1}^c, B_t)$ 
    Synchronize shared blocks  $\theta_{t,[m] \setminus A}^{c,A} = \theta_{t,[m] \setminus A}^c$ 
end for

```

Throughout this process, each skewed counterfactually trained block progressively adapts to the neighboring clean blocks to classify skewed data. By design, all blocks receive the same exposure to training data, with the only difference being the presence or the absence of a skew. The training algorithm remains consistent across all blocks, controlling for the optimizer’s implicit biases and satisfying our desiderata.

## 4 EXPERIMENT DETAILS

**Datasets and Skews** We consider three datasets with distinct skews: CIFAR-10 (Krizhevsky, 2009) with *watermark skew*, Waterbirds (Sagawa\* et al., 2020) with *background skew*, and CelebA (Liu et al., 2015) with *group sampling skew* (Sagawa\* et al., 2020). For the watermark skew (see Figure 1), we blend the upper-left corner of CIFAR images with class-correlated MNIST (Lecun et al., 1998) digits, encouraging the network to rely on the simple MNIST watermark. For the background skew, following Sagawa\* et al. (2020), we place bird images on class-correlated backgrounds, incentivizing the reliance on background cues. For the sampling skew, we sample the skewed dataset introducing a correlation between gender and hair color, encouraging demographic shortcuts.

We generate skews using the following procedure. First, we create a clean dataset where the considered skew is not predictive. For CIFAR and Waterbirds, we simply match each image with a random image of MNIST digit or background, respectively. For CelebA, we remove some images of blond females, non-blond males, and non-blond females to balance

groups.<sup>2</sup> Then, we create a *fully skewed dataset* where the considered skew is perfectly predictive of the label. For CIFAR and Waterbirds, we replace a previously matched random image with an image corresponding to the image label if the class of random image does not already correspond to the image label. For CelebA, we replace the images of blonde males with blonde females and the images of non-blonde females with non-blond males, making spurious correlation perfectly predictive. Finally, we create a skewed dataset, where each clean image is replaced with a corresponding fully skewed image with a certain frequency. We consider two frequencies: *common* and *rare* (127/128 and 15/16, respectively). For CIFAR, we use watermarks of size  $10 \times 10$  and two blending strengths *strong* and *weak*, which equal to 3/4 and 1/4, respectively.

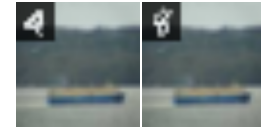


Figure 1: Clean (left) and skewed (right) CIFAR-10 image of class 8 with MNIST watermark

**Models and Optimizers** We consider four architectures: VGG-11 (Simonyan and Zisserman, 2015), a typical convolutional neural network (CNN); ResNet-18 (He et al., 2016), a CNN with residual connections; DeiT-Ti (Touvron et al., 2021), a vision transformer (ViT); and ConvNeXt-T (Liu et al., 2022), a modernized CNN. Since all tasks have few classes, we use global average pooling instead of dense classification layers in VGG-11. We decompose each architecture into 6 blocks. The first block always corresponds to the initial convolutional layer, while the last block corresponds to the final linear layer. For the rest, we do the following. For VGG, we use max-pool layers as block boundaries. For ResNet and ConvNeXt, we use convolutional layers with stride 2 as boundaries (see Figure 3 in He et al., 2016). For DeiT, we divide the rest into four equal blocks. We consider SGD (Robbins and Monro, 1951) and AdamW (Loshchilov and Hutter, 2019) optimizers, and either train from scratch or fine-tune from ImageNet (Deng et al., 2009) initialization. (See Section C for details.)

**Experiment Scope** We conduct two types of experiments. First, using intervention sets  $A = [m] \setminus \{i\}$ , we assess whether shortcuts could be localized in a single block by testing whether a *single block’s contribution* to could fully explain them, i.e.,  $\exists i : \frac{\text{fgt}_i}{\text{er}(\theta^s) - \text{er}(\theta^c)} \approx$

<sup>2</sup>The final number of blond and non-blond images equals to the number of blond females and non-blond males in the original dataset

$1 \vee \frac{\text{enc}_i}{\text{er}(\theta^s) - \text{er}(\theta^c)} \approx 1$ . Second, to quantify layer-wise contributions, using intervention sets  $A = i : m$ , we measure the *rate of increase in relative contributions of initial blocks*’ to forgetting and encoding,

$$\frac{\text{fgt}_{0:i+1} - \text{fgt}_{0:i}}{\text{er}(\theta^s) - \text{er}(\theta^c)} \quad \text{and} \quad \frac{\text{enc}_{0:i+1} - \text{enc}_{0:i}}{\text{er}(\theta^s) - \text{er}(\theta^c)}.$$

## 5 RESULTS

This section presents the results of our experiments for fine-tuned models (see training from scratch results in Section B). First, we compute the localization metrics for individual and initial blocks. Then, we analyze which factors contribute the most to the localization in the initial blocks. Finally, we investigate whether our localization metrics are predictive of the success of layer-wise training interventions.

To understand the extent of shortcut learning, Table 1 presents the clean test dataset error rates achieved by the models fine-tuned with AdamW on clean and skewed data for our datasets (SGD behavior is similar). We repeat each experiment 5 times to average over training noise and report the averaged values and their standard errors with the Bessel’s correction.

### 5.1 Localization of Encoding and Forgetting

**Localization in a Single Block** Table 2 presents the relative individual contributions of blocks for the models fine-tuned with AdamW on the CIFAR-10 (strong) dataset with common skew. First, no single block achieves 100% relative contribution to encoding or forgetting (according to the 5% critical value for one sided t-test). Moreover, there is no individual block whose contribution is much larger than the contributions of other blocks. Second, the sum of individual contributions generally either significantly (according to the 5% critical value for the two-sided t-test) exceeds 100% (for encoding, with an exception of VGG-11 model) or does not reach 100% (for forgetting), suggesting that simply analyzing individual block contributions without interactions between them generally does not lead to accurate analysis.

Our findings suggest that shortcut learning is not concentrated in any single block. The interactions between layers seem crucial for shortcut emergence, suggesting that shortcut learning cannot be easily decomposed into a sum of individual layer contributions. Similar patterns emerge across all experimental settings (see additional results in Section A). For single-block localization and fine-tuning, we discovered a rare possibility of model divergence (when the model achieves a higher error rate than the skewed model

on clean data and a higher error rate than the clean model on skewed data). Divergences occurred in only 7 (out of 3840) intervened models (and only in the single block setting). Such models were excluded from the analysis without impacting our conclusions.

**Localization in the Initial Blocks** To account for layer interactions, we examined intervention sets  $A = i : m$ . Table 6 presents the results for models fine-tuned with AdamW on common skews. To make the results comparable, we report the rate of increase in relative contributions. As expected, encoding and forgetting generally increase with the number of layers involved. All architectures first encode spurious features and subsequently forget core features. The last layer plays a major role in feature forgetting, while the first layer has minimal contributions.<sup>3</sup>

These results indicate that shortcut learning indeed consists of two processes that occur in different layers. First, the network encodes spurious features; then, due to predictive spurious features, it progressively forgets core features, leading to a shortcut classification rule.

### 5.2 Differences in Relative Contributions

**Main Explanatory Factors** Table 4 reports the fraction of the total variance of the increase rate of relative encoding and forgetting explained by different factors. Dataset and model architecture are the most predictive factors for encoding localization, while skew frequency and optimizer choice are the most predictive for forgetting localization. Together, dataset and model factors explain 83.8% of variance in encoding localization, while skew frequency and optimizer factors explain 57.0% of variance in forgetting localization.

These findings suggest that encoding localization is primarily driven by the skew’s semantic properties: the dataset is directly related to it, while the architecture determines the abstraction levels of layers. At the same time, forgetting appears to be primarily influenced by the skew’s predictive power (through the dataset and skew frequency) and the implicit biases of optimizer. We further explore these factors below.

**Differences in Encoding** Table 6 (top part) shows the increase rate in relative encoding for models fine-tuned with AdamW on common skews. Watermark skew tends to be encoded earlier, while sampling skew is typically encoded in later layers. Additionally, CNN architectures generally encode spurious features in the latter layers compared to ViT architectures.

<sup>3</sup>For the training from scratch, the first layer starts to engage in spurious feature encoding, Table 15 in Appendix.

Table 1: Average clean test error rates (and their standard errors in parenthesis) of clean and skewed models fine-tuned with AdamW for rare (top part) and common (bottom part) skews

Model	CIFAR-10 (weak)		CIFAR-10 (strong)		Waterbirds		CelebA	
	Clean	Skewed	Clean	Skewed	Clean	Skewed	Clean	Skewed
DeiT-Ti	3.2% (0.1%)	5.2% (0.1%)	3.4% (0.1%)	8.6% (0.1%)	2.0% (0.1%)	9.4% (0.4%)	5.8% (0.1%)	11.3% (0.2%)
ResNet-18	4.1% (0.1%)	7.2% (0.1%)	4.3% (0.1%)	11.5% (0.2%)	2.1% (0.1%)	8.5% (0.3%)	5.9% (0.1%)	11.3% (0.3%)
VGG-11	6.9% (0.1%)	17.1% (0.3%)	7.2% (0.1%)	26.3% (0.2%)	2.5% (0.1%)	10.7% (0.2%)	6.0% (0.1%)	11.0% (0.3%)
ConvNext-T	1.8% (0.1%)	3.3% (0.1%)	1.9% (0.1%)	5.1% (0.1%)	0.8% (0.1%)	3.7% (0.2%)	5.8% (0.1%)	11.4% (0.2%)
DeiT-Ti	3.2% (0.1%)	7.8% (0.2%)	3.4% (0.1%)	17.5% (0.3%)	2.0% (0.1%)	19.9% (0.6%)	5.8% (0.1%)	20.4% (0.8%)
ResNet-18	4.1% (0.1%)	11.3% (0.3%)	4.3% (0.1%)	25.3% (0.3%)	2.1% (0.1%)	18.2% (0.2%)	5.9% (0.1%)	19.4% (0.4%)
VGG-11	6.9% (0.1%)	29.2% (0.5%)	7.2% (0.1%)	52.4% (0.4%)	2.5% (0.1%)	25.3% (0.4%)	6.0% (0.1%)	21.3% (0.7%)
ConvNext-T	1.8% (0.1%)	5.4% (0.1%)	1.9% (0.1%)	11.6% (0.2%)	0.8% (0.1%)	10.9% (0.5%)	5.8% (0.1%)	20.8% (0.7%)

**Differences in Forgetting** Table 3 presents the increase rate in relative forgetting for DeiT-Ti models fine-tuned on the CIFAR-10 (strong) dataset. SGD prioritizes forgetting in the last layer, whereas AdamW primary distributes it between the last layer and the penultimate block. Simultaneously, forgetting due to common skews is relatively more concentrated in the last layer compared to one induced by rare skews.

### 5.3 Localization-Guided Interventions

This section explores whether our localization metrics can predict the success of shortcut mitigation strategies. We retrained DeiT-Ti, ResNet-18, and VGG-11 with AdamW on skewed data, using common skews in Waterbirds, CelebA, and CIFAR-10 (strong). We consider four retraining interventions, where we modify the hyperparameters of the optimizer layer-wise: 1–2) increasing or decreasing LR (learning rate) by a factor of 3, and 3–4) increasing or decreasing WD (weight decay) by a factor of 10. We applied these interventions to individual blocks and the groups of two consecutive blocks. Then, we regressed the extent of shortcut mitigation (the difference in test accuracy on clean data between skewed retrained and non-intervened models normalized against the same difference between non-intervened skewed and clean models), on encoding and forgetting metrics (from Table 6), their interaction (i.e., a product of these metrics), their squares, and dummies for the first and last layer, and double layer intervention. Additionally, we conduct an experiment

where we train the last layer and then the whole network for a short time, and then freeze all blocks except one during fine-tuning.

Table 5 presents the results for the relevancy of our metrics (expressed through the F-statistic (Greene, 2003) for the joint significance of the five metric-related coefficients) and overall predictive power of the regression (expressed through  $R^2$ ).<sup>4</sup> Our localization metrics are predictive of success for LR and freezing interventions (on a 5% significance level). This finding suggests that our localization metrics capture relevant information and could inform shortcut mitigations.

## 6 DISCUSSION

We analyzed the localization of shortcuts in deep models. We decomposed shortcut learning into two fundamental processes: spurious feature promotion and core feature degradation. Using our counterfactual retraining method, we examined them through two metrics: spurious feature encoding and core feature forgetting.

Our findings demonstrate that neither encoding nor forgetting is localized in any single layer within vision models. The interactions between layers play a crucial role in shortcut formation. Earlier blocks typically facilitate spurious feature encoding, while latter blocks are responsible for core feature forgetting.

<sup>4</sup>see Table 7 in Appendix for regression coefficients

Table 2: Average relative contributions (and standard errors) of single blocks to encoding (top) and forgetting (bottom) for models fine-tuned with AdamW on CIFAR-10 (strong) with common skew

Model	Bl. 0	Bl. 1	Bl. 2	Bl. 3	Bl. 4	Bl. 5
DeiT-Ti	0.1%	33.5%	42.9%	48.8%	25.4%	0.1%
	(1.7%)	(2.2%)	(2.0%)	(0.9%)	(2.3%)	(1.7%)
ResNet-18	2.4%	9.8%	16.9%	46.1%	66.0%	2.7%
	(1.2%)	(1.0%)	(1.4%)	(0.6%)	(0.5%)	(0.7%)
VGG-11	-0.5%	-0.2%	12.0%	53.0%	39.8%	4.1%
	(0.3%)	(0.2%)	(0.8%)	(1.7%)	(2.6%)	(0.5%)
ConvNext-T	-1.9%	4.5%	13.2%	76.4%	44.1%	0.1%
	(3.5%)	(1.3%)	(3.0%)	(1.2%)	(0.7%)	(1.6%)
DeiT-Ti	0.7%	1.0%	0.8%	0.4%	0.6%	-0.2%
	(0.5%)	(0.4%)	(0.6%)	(0.4%)	(1.0%)	(0.4%)
ResNet-18	0.2%	0.6%	1.8%	2.7%	5.1%	0.3%
	(0.4%)	(0.3%)	(0.4%)	(0.6%)	(0.2%)	(0.2%)
VGG-11	-0.1%	0.2%	0.8%	10.0%	9.7%	0.3%
	(0.3%)	(0.3%)	(0.3%)	(1.4%)	(1.7%)	(0.2%)
ConvNext-T	-0.4%	1.0%	0.8%	1.6%	1.0%	-0.6%
	(0.9%)	(1.0%)	(0.8%)	(0.7%)	(0.8%)	(0.6%)

Table 3: Relative forgetting rate (and standard errors) of DeiT-Ti models fine-tuned on CIFAR-10 (strong)

Frequency	Optimizer	Bl. 0	Bl. 1	Bl. 2	Bl. 3	Bl. 4	Bl. 5
Rare	AdamW	0.1%	3.2%	5.0%	8.4%	19.8%	63.7%
		(2.2%)	(0.8%)	(1.3%)	(1.7%)	(2.0%)	(1.8%)
	SGD	0.3%	4.4%	4.0%	9.1%	11.0%	71.6%
		(1.4%)	(1.0%)	(1.0%)	(0.5%)	(0.9%)	(1.2%)
Common	AdamW	0.6%	1.1%	1.9%	5.2%	11.0%	80.6%
		(0.5%)	(0.5%)	(0.4%)	(0.2%)	(0.5%)	(0.8%)
	SGD	0.2%	1.9%	1.9%	5.1%	6.7%	84.5%
		(0.2%)	(0.4%)	(0.4%)	(0.6%)	(0.6%)	(0.9%)

Table 4: Variance explained in relative encoding (top) and forgetting (bottom) rate by different factors

Dataset	Skew freq.	Model	Optimizer
45.7%	0.4%	26.3%	3.3%
14.7%	21.0%	9.1%	33.5%

**Practical Implications for Fine-tuning** Examining the axes of variation in our metrics, we found that dataset and model architecture play a crucial role in the localization of encoding, while skew frequency and optimizer are important for forgetting. Additionally, our localization metrics are predictive of the success of some layer-wise interventions. These results jointly suggest that shortcut mitigations based on layer-wise manipulation of learning rates and frozen layers (e.g., Lee et al., 2023) should be dataset- and architecture-specific.

Table 5: Predictive power of localization metrics

	LR $\uparrow$	LR $\downarrow$	WD $\uparrow$	WD $\downarrow$	Freeze
F-Stat	5.04	8.76	0.66	0.44	4.07
R $^2$	0.36	0.54	0.07	0.05	0.32
N	99	99	99	99	54

**Future Work** We hope our results will facilitate future research on developing more robust models that can effectively resist spurious correlations.

Specifically, our observations suggest a trade-off between feature extractor adaptability and robustness, which would be interesting to study in the future. Feature extractors trained on clean data provide greater robustness against shortcuts by compelling the final classifier layers to utilize core features. However, models with clean feature extractors have higher error rate on fully skewed datasets (see Table 8 in Appendix).

Table 6: Average increase rate in relative contributions (and standard errors) of the initial blocks to encoding (top part) and forgetting (bottom part) for models fine-tuned with AdamW on common skews

Dataset	Model	Bl. 0	Bl. 1	Bl. 2	Bl. 3	Bl. 4	Bl. 5
CIFAR-10 (strong)	DeiT-Ti	1.1% (3.1%)	40.3% (2.0%)	39.5% (1.8%)	15.1% (0.7%)	4.3% (0.4%)	0.1% (0.1%)
	ResNet-18	2.4% (1.2%)	10.5% (1.0%)	26.1% (1.4%)	45.6% (0.8%)	15.7% (0.6%)	0.1% (0.1%)
	VGG-11	-0.5% (0.3%)	1.5% (0.2%)	17.8% (0.3%)	72.3% (0.2%)	9.1% (0.3%)	0.0% (0.1%)
	ConvNext-T	-1.8% (3.8%)	6.7% (5.3%)	24.6% (2.1%)	67.6% (1.9%)	3.3% (0.2%)	-0.1% (0.2%)
Waterbirds	DeiT-Ti	1.2% (2.4%)	19.1% (2.5%)	30.3% (2.8%)	24.6% (1.8%)	25.0% (1.1%)	0.0% (0.1%)
	ResNet-18	6.7% (1.5%)	11.7% (1.1%)	18.9% (1.0%)	27.2% (0.9%)	35.4% (1.0%)	0.4% (0.3%)
	VGG-11	4.5% (0.9%)	9.8% (2.8%)	18.9% (1.8%)	51.6% (1.8%)	14.9% (0.9%)	0.6% (0.2%)
	ConvNext-T	7.2% (2.2%)	2.6% (4.8%)	15.0% (3.6%)	62.4% (2.2%)	13.0% (1.6%)	0.2% (0.2%)
CelebA	DeiT-Ti	2.0% (0.7%)	5.1% (2.1%)	8.7% (1.4%)	18.5% (0.6%)	58.9% (2.1%)	7.2% (0.6%)
	ResNet-18	0.7% (1.7%)	-3.2% (1.4%)	9.2% (0.7%)	23.0% (1.8%)	64.5% (1.7%)	6.2% (1.4%)
	VGG-11	4.1% (0.6%)	1.5% (0.6%)	7.1% (1.3%)	27.7% (1.9%)	60.0% (2.3%)	0.1% (0.4%)
	ConvNext-T	-0.7% (1.7%)	3.0% (1.2%)	3.0% (1.7%)	18.1% (2.2%)	59.4% (2.0%)	17.5% (1.0%)
CIFAR-10 (strong)	DeiT-Ti	0.6% (0.5%)	1.1% (0.5%)	1.9% (0.4%)	5.2% (0.2%)	11.0% (0.5%)	80.6% (0.8%)
	ResNet-18	0.2% (0.4%)	0.9% (0.3%)	1.8% (0.4%)	2.0% (0.4%)	19.3% (0.7%)	76.1% (0.5%)
	VGG-11	-0.1% (0.3%)	0.2% (0.2%)	0.7% (0.2%)	2.2% (0.3%)	21.7% (0.3%)	75.7% (0.5%)
	ConvNext-T	-0.2% (0.8%)	1.6% (0.6%)	-0.4% (0.3%)	5.1% (0.6%)	13.5% (0.9%)	80.7% (0.9%)
Waterbirds	DeiT-Ti	0.7% (0.4%)	0.5% (0.2%)	1.9% (0.5%)	5.6% (0.4%)	23.0% (0.9%)	68.6% (0.9%)
	ResNet-18	0.6% (0.4%)	1.1% (0.2%)	0.5% (0.4%)	2.5% (0.6%)	28.6% (3.0%)	67.0% (3.2%)
	VGG-11	0.3% (0.3%)	0.2% (0.3%)	-0.2% (0.5%)	2.8% (0.7%)	29.8% (1.0%)	67.3% (1.0%)
	ConvNext-T	0.6% (0.3%)	0.5% (0.6%)	0.5% (0.3%)	2.2% (0.2%)	16.6% (0.6%)	79.8% (0.6%)
CelebA	DeiT-Ti	0.0% (0.1%)	0.4% (0.4%)	2.2% (0.5%)	2.1% (0.5%)	10.9% (0.7%)	84.7% (1.1%)
	ResNet-18	-0.2% (0.4%)	0.1% (0.2%)	1.0% (0.4%)	3.3% (0.7%)	15.9% (1.0%)	80.2% (0.7%)
	VGG-11	0.1% (0.3%)	0.4% (0.2%)	1.9% (0.2%)	4.6% (0.8%)	26.5% (2.4%)	66.9% (1.7%)
	ConvNext-T	-0.3% (0.3%)	-0.0% (0.3%)	-0.0% (0.2%)	2.0% (0.4%)	10.7% (0.6%)	87.9% (1.1%)

## Acknowledgments

This research was partially funded from the Ministry of Education and Science of Bulgaria (support for IN-SAIT, part of the Bulgarian National Roadmap for Research Infrastructure). This project was supported with computational resources provided by Google Cloud Platform (GCP).

## References

Abbe, E., Adsera, E. B., and Misiakiewicz, T. (2022). The merged-staircase property: a necessary and nearly sufficient condition for SGD learning of sparse functions on two-layer neural networks. In Loh, P.-L. and Raginsky, M., editors, *Proceedings of Thirty Fifth Conference on Learning Theory*, volume 178 of *Proceedings of Machine Learning Research*, pages 4782–4887. PMLR.

Allen-Zhu, Z. and Li, Y. (2019). What Can ResNet Learn Efficiently, Going Beyond Kernels? In Wallach, H., Larochelle, H., Beygelzimer, A., d’Alché-Buc, F., Fox, E., and Garnett, R., editors, *Advances in Neural Information Processing Systems*, volume 32. Curran Associates, Inc.

Arjovsky, M., Bottou, L., Gulrajani, I., and Lopez-Paz, D. (2020). Invariant Risk Minimization. arXiv:1907.02893 [stat.ML].

Brunet, M.-E., Anderson, A., and Zemel, R. (2022). Implications of Model Indeterminacy for Explanations of Automated Decisions. In Koyejo, S., Mohamed, S., Agarwal, A., Belgrave, D., Cho, K., and Oh, A., editors, *Advances in Neural Information Processing Systems*, volume 35, pages 7810–7823. Curran Associates, Inc.

Chaudhuri, K., Ahuja, K., Arjovsky, M., and Lopez-Paz, D. (2023). Why does Throwing Away Data Improve Worst-Group Error? In Krause, A., Brunskill, E., Cho, K., Engelhardt, B., Sabato, S., and Scarlett, J., editors, *Proceedings of the 40th International Conference on Machine Learning*, volume 202 of *Proceedings of Machine Learning Research*, pages 4144–4188. PMLR.

Deng, J., Dong, W., Socher, R., Li, L.-J., Li, K., and Fei-Fei, L. (2009). ImageNet: A large-scale hierarchical image database. In *2009 IEEE Conference on Computer Vision and Pattern Recognition*, pages 248–255.

Geirhos, R., Jacobsen, J.-H., Michaelis, C., Zemel, R., Brendel, W., Bethge, M., and Wichmann, F. A. (2020). Shortcut learning in deep neural networks. *Nature Machine Intelligence*, 2(11):665–673.

Greene, W. H. (2003). Econometric analysis. *Pretence Hall*.

He, K., Zhang, X., Ren, S., and Sun, J. (2016). Deep Residual Learning for Image Recognition. In *Proceedings of the IEEE Conference on Computer Vision and Pattern Recognition (CVPR)*.

Hermann, K. and Lampinen, A. (2020). What shapes feature representations? exploring datasets, architectures, and training. In Larochelle, H., Ranzato, M., Hadsell, R., Balcan, M., and Lin, H., editors, *Advances in Neural Information Processing Systems*, volume 33, pages 9995–10006. Curran Associates, Inc.

Huh, M., Mobahi, H., Zhang, R., Cheung, B., Agrawal, P., and Isola, P. (2023). The Low-Rank Simplicity Bias in Deep Networks. *Transactions on Machine Learning Research*.

Islam, M. A., Kowal, M., Esser, P., Jia, S., Ommer, B., Derpanis, K. G., and Bruce, N. (2021). Shape or Texture: Understanding Discriminative Features in CNNs. In *International Conference on Learning Representations*.

Kirichenko, P., Izmailov, P., and Wilson, A. G. (2023). Last Layer Re-Training is Sufficient for Robustness to Spurious Correlations. In *The Eleventh International Conference on Learning Representations*.

Krizhevsky, A. (2009). Learning Multiple Layers of Features from Tiny Images.

Kumar, A., Raghunathan, A., Jones, R. M., Ma, T., and Liang, P. (2022). Fine-Tuning can Distort Pretrained Features and Underperform Out-of-Distribution. In *International Conference on Learning Representations*.

Lecun, Y., Bottou, L., Bengio, Y., and Haffner, P. (1998). Gradient-based learning applied to document recognition. *Proceedings of the IEEE*, 86(11):2278–2324.

Lee, Y., Chen, A. S., Tajwar, F., Kumar, A., Yao, H., Liang, P., and Finn, C. (2023). Surgical Fine-Tuning Improves Adaptation to Distribution Shifts. In *The Eleventh International Conference on Learning Representations*.

Lewkowycz, A., Bahri, Y., Dyer, E., Sohl-Dickstein, J., and Gur-Ari, G. (2020). The large learning rate phase of deep learning: the catapult mechanism. arXiv:2003.02218 [stat.ML].

Li, Y., Wei, C., and Ma, T. (2019). Towards Explaining the Regularization Effect of Initial Large Learning Rate in Training Neural Networks. In Wallach, H., Larochelle, H., Beygelzimer, A., d’Alché-Buc, F., Fox, E., and Garnett, R., editors, *Advances in Neural Information Processing Systems*, volume 32. Curran Associates, Inc.

Liu, Z., Luo, P., Wang, X., and Tang, X. (2015). Deep Learning Face Attributes in the Wild. In *Proceedings of the IEEE International Conference on Computer Vision (ICCV)*.

Liu, Z., Mao, H., Wu, C.-Y., Feichtenhofer, C., Darrell, T., and Xie, S. (2022). A ConvNet for the 2020s. In *Proceedings of the IEEE/CVF Conference on Computer Vision and Pattern Recognition (CVPR)*, pages 11976–11986.

Loshchilov, I. and Hutter, F. (2019). Decoupled Weight Decay Regularization. In *International Conference on Learning Representations*.

Maini, P., Mozer, M. C., Sedghi, H., Lipton, Z. C., Kolter, J. Z., and Zhang, C. (2023). Can Neural Network Memorization Be Localized? In Krause, A., Brunskill, E., Cho, K., Engelhardt, B., Sabato, S., and Scarlett, J., editors, *Proceedings of the 40th International Conference on Machine Learning*, volume 202 of *Proceedings of Machine Learning Research*, pages 23536–23557. PMLR.

Nagarajan, V., Andreassen, A., and Neyshabur, B. (2021). Understanding the failure modes of out-of-distribution generalization. In *International Conference on Learning Representations*.

Panigrahi, A., Liu, B., Malladi, S., Risteski, A., and Goel, S. (2024). Progressive distillation improves feature learning via implicit curriculum. In *ICML 2024 Workshop on Mechanistic Interpretability*.

Puli, A., Zhang, L., Wald, Y., and Ranganath, R. (2023). Don’t blame Dataset Shift! Shortcut Learning due to Gradients and Cross Entropy. In Oh, A., Naumann, T., Globerson, A., Saenko, K., Hardt, M., and Levine, S., editors, *Advances in Neural Information Processing Systems*, volume 36, pages 71874–71910. Curran Associates, Inc.

Robbins, H. and Monro, S. (1951). A Stochastic Approximation Method. *The Annals of Mathematical Statistics*, 22(3):400–407.

Sagawa\*, S., Koh\*, P. W., Hashimoto, T. B., and Liang, P. (2020). Distributionally Robust Neural Networks. In *International Conference on Learning Representations*.

Sagawa, S., Raghunathan, A., Koh, P. W., and Liang, P. (2020). An Investigation of Why Overparameterization Exacerbates Spurious Correlations. In III, H. D. and Singh, A., editors, *Proceedings of the 37th International Conference on Machine Learning*, volume 119 of *Proceedings of Machine Learning Research*, pages 8346–8356. PMLR.

Scimeca, L., Oh, S. J., Chun, S., Poli, M., and Yun, S. (2022). Which Shortcut Cues Will DNNs Choose? A Study from the Parameter-Space Perspective. In *International Conference on Learning Representations*.

Shah, H., Tamuly, K., Raghunathan, A., Jain, P., and Netrapalli, P. (2020). The Pitfalls of Simplicity Bias in Neural Networks. In Larochelle, H., Ranzato, M., Hadsell, R., Balcan, M., and Lin, H., editors, *Advances in Neural Information Processing Systems*, volume 33, pages 9573–9585. Curran Associates, Inc.

Simonyan, K., Vedaldi, A., and Zisserman, A. (2014). Deep Inside Convolutional Networks: Visualising Image Classification Models and Saliency Maps. arXiv:1312.6034 [cs.CV].

Simonyan, K. and Zisserman, A. (2015). Very Deep Convolutional Networks for Large-Scale Image Recognition. In *International Conference on Learning Representations*.

TorchVision maintainers and contributors (2016). TorchVision: PyTorch’s Computer Vision library.

Touvron, H., Cord, M., Douze, M., Massa, F., Sablayrolles, A., and Jegou, H. (2021). Training data-efficient image transformers & distillation through attention. In Meila, M. and Zhang, T., editors, *Proceedings of the 38th International Conference on Machine Learning*, volume 139 of *Proceedings of Machine Learning Research*, pages 10347–10357. PMLR.

Trivedi, P., Koutra, D., and Thiagarajan, J. J. (2023). A Closer Look at Model Adaptation using Feature Distortion and Simplicity Bias. In *The Eleventh International Conference on Learning Representations*.

Tsoy, N. and Konstantinov, N. (2024). Simplicity Bias of Two-Layer Networks beyond Linearly Separable Data. In *Forty-first International Conference on Machine Learning*.

Wah, C., Branson, S., Welinder, P., Perona, P., and Belongie, S. (2011). The Caltech-UCSD Birds-200-2011 Dataset. Technical Report CNS-TR-2011-001, California Institute of Technology.

Wang, S., Veldhuis, R., Brune, C., and Strisciuglio, N. (2023). What do neural networks learn in image classification? a frequency shortcut perspective. In *Proceedings of the IEEE/CVF International Conference on Computer Vision (ICCV)*, pages 1433–1442.

Wightman, R. (2019). PyTorch Image Models.

Zhang, C., Bengio, S., and Singer, Y. (2022). Are All Layers Created Equal? *Journal of Machine Learning Research*, 23(67):1–28.

Zhou, B., Lapedriza, A., Khosla, A., Oliva, A., and Torralba, A. (2017). Places: A 10 million Image

Database for Scene Recognition. *IEEE Transactions on Pattern Analysis and Machine Intelligence*.

Zhu, H., Chen, B., and Yang, C. (2023). Understanding Why ViT Trains Badly on Small Datasets: An Intuitive Perspective. arXiv:2302.03751 [cs.CV].

---

## Supplementary Material

---

<b>A ADDITIONAL RESULTS FOR FINE-TUNED MODELS</b>	<b>12</b>
<b>B TRAINING FROM SCRATCH</b>	<b>16</b>
<b>C DETAILS OF TRAINING</b>	<b>20</b>
<b>D MISCELLANEOUS</b>	<b>23</b>
D.1 Licenses of the Used Assets . . . . .	23

### A ADDITIONAL RESULTS FOR FINE-TUNED MODELS

**Localization-Guided Interventions** Table 7 present the full version of Table 5.

Table 7: Predictive power of localization metrics with regression coefficients (and their standard errors)

	LR↑	LR↓	WD↑	WD↓	Freeze
Enc	−0.35 (0.11)	0.20 (0.07)	−0.02 (0.02)	−0.02 (0.02)	−1.36 (0.92)
Fgt	0.39 (0.11)	−0.45 (0.09)	0.01 (0.02)	0.01 (0.02)	5.16 (1.31)
Enc × Fgt	0.14 (0.11)	0.13 (0.10)	0.00 (0.02)	0.01 (0.02)	−6.25 (3.18)
Enc <sup>2</sup>	0.21 (0.14)	−0.11 (0.08)	0.01 (0.02)	0.02 (0.02)	2.25 (1.57)
Fgt <sup>2</sup>	−0.12 (0.14)	−0.06 (0.14)	−0.00 (0.02)	−0.01 (0.03)	−6.96 (2.20)
First	−0.03 (0.02)	0.03 (0.02)	−0.00 (0.01)	−0.00 (0.01)	0.12 (0.17)
Last	−0.22 (0.08)	0.34 (0.08)	−0.01 (0.02)	−0.00 (0.02)	0.12 (0.92)
Const	−0.01 (0.02)	−0.02 (0.01)	0.00 (0.01)	0.00 (0.01)	−0.22 (0.13)
Double	0.02 (0.02)	−0.01 (0.01)	0.00 (0.01)	0.00 (0.01)	
F-Stat	5.04	8.76	0.66	0.44	4.07
R <sup>2</sup>	0.36	0.54	0.07	0.05	0.32
N	99	99	99	99	54

**Error Rates on Fully Skewed Dataset** Table 8 presents error rates of the clean models intervened with sets  $A = i : m$  for AdamW fine-tuned architectures on CIFAR-10 (strong) with common skew. As we can see, the error rates increase with the number of initial clean blocks.

**Additional Results on Localization in a Single Block** Table 9 follows Table 2 for the models fine-tuned with AdamW on CelebA and Waterbirds with common skew. Similarly to the CIFAR-10 results, there does not

Table 8: Average test error rates (and standard errors) on the fully skewed CIFAR-10 (strong) dataset of clean models intervened with sets  $A = i : m$  for AdamW fine-tuned architectures on common skew

Model	Skewed	1 : 6	2 : 6	3 : 6	4 : 6	5 : 6	Clean
DeiT-Ti	0.3% (0.1%)	0.3% (0.1%)	0.5% (0.1%)	1.3% (0.1%)	2.3% (0.1%)	3.4% (0.1%)	3.4% (0.1%)
ResNet-18	0.3% (0.1%)	0.3% (0.1%)	0.3% (0.1%)	0.4% (0.1%)	1.3% (0.1%)	4.2% (0.1%)	4.2% (0.1%)
VGG-11	0.3% (0.1%)	0.3% (0.1%)	0.3% (0.1%)	0.3% (0.1%)	2.4% (0.1%)	7.2% (0.1%)	7.2% (0.1%)

exist an individual layer fully responsible for shortcut learning. As previously, the sum of individual contributions to forgetting does not reach 100%, which suggest that forgetting can not be explained by the sum of individual contributions. In contrast to the previous results, the sum of individual contributions to encoding does not reach 100% for CelebA and approximately equals 100% for Waterbirds. These results again suggest that the sum of individual contributions can not reliably explain spurious feature encoding. While this approach gives plausible results for the Waterbirds dataset, it fails for the CIFAR-10 and CelebA datasets.

Interestingly, Block 4 of the VGG-11 model exhibits a strong negative contribution to encoding. To understand this behavior, we examined the individual contributions to encoding for the same models trained on rare skew in Table 10 and the error rates of these models in Table 11. Similarly to the common skew, Block 4 of the VGG-11 model exhibits a strong negative contribution to encoding. Also, all intervened models achieve a small error rate on the fully skewed dataset. A plausible explanation of this behavior is the following. Block 4 in the clean model is not well suited for spurious feature encoding. Due to regularization (i.e., implicit biases of optimizer and weight decay), the complement to this block can not overcome this restriction and starts to mix core features with spurious features, which corrupts the core features and leads to a significant accuracy drop on the clean dataset. This example again suggests that shortcut learning crucially depends on the interactions of different layers within the network.

Table 9: Average relative contributions (and standard errors) of single blocks to encoding (first and third sub-part) and forgetting (second and fourth sub-parts) for models fine-tuned with AdamW on CelebA (top part) and Waterbirds (bottom part) with common skew

Model	Bl. 0	Bl. 1	Bl. 2	Bl. 3	Bl. 4	Bl. 5
DeiT-Ti	2.0%	3.7%	6.6%	-0.1%	2.1%	0.7%
	(0.7%)	(1.9%)	(1.9%)	(1.5%)	(1.3%)	(0.6%)
ResNet-18	0.7%	-1.4%	0.7%	-11.7%	12.1%	-0.1%
	(1.7%)	(5.9%)	(3.1%)	(3.2%)	(5.6%)	(1.0%)
VGG-11	4.1%	3.2%	4.9%	5.0%	-73.3%	-4.3%
	(0.6%)	(1.0%)	(2.4%)	(6.8%)	(10.6%)	(0.7%)
ConvNeXt-Ti	0.2%	2.6%	2.2%	9.8%	-0.4%	-2.6%
	(1.8%)	(1.7%)	(2.3%)	(3.6%)	(2.6%)	(1.1%)
DeiT-Ti	0.0%	0.2%	0.9%	0.5%	0.2%	0.0%
	(0.1%)	(0.2%)	(0.2%)	(0.2%)	(0.3%)	(0.2%)
ResNet-18	-0.2%	0.8%	0.4%	2.3%	23.8%	-0.1%
	(0.4%)	(0.5%)	(0.3%)	(0.4%)	(13.6%)	(0.2%)
VGG-11	0.1%	0.3%	1.7%	7.9%	0.6%	-0.1%
	(0.3%)	(0.3%)	(0.7%)	(2.2%)	(0.7%)	(0.3%)
ConvNeXt-Ti	-0.0%	-0.4%	-0.2%	1.4%	0.1%	-0.0%
	(0.3%)	(0.2%)	(0.4%)	(0.7%)	(0.5%)	(0.2%)
DeiT-Ti	1.2%	16.7%	32.4%	31.2%	14.8%	3.2%
	(2.4%)	(2.1%)	(4.8%)	(2.4%)	(2.6%)	(1.5%)
ResNet-18	6.7%	12.4%	24.8%	40.7%	17.0%	1.4%
	(1.5%)	(1.8%)	(1.9%)	(3.5%)	(7.0%)	(0.5%)
VGG-11	4.5%	10.2%	31.3%	64.3%	18.9%	2.0%
	(0.9%)	(2.9%)	(0.6%)	(2.3%)	(4.7%)	(0.5%)
ConvNeXt-Ti	-3.1%	2.4%	12.7%	77.7%	51.3%	1.7%
	(5.3%)	(2.0%)	(4.7%)	(3.1%)	(1.3%)	(4.7%)
DeiT-Ti	0.7%	0.7%	1.1%	1.8%	0.9%	0.1%
	(0.4%)	(0.4%)	(0.3%)	(0.4%)	(0.4%)	(0.4%)
ResNet-18	0.6%	0.5%	0.7%	1.1%	20.7%	0.1%
	(0.4%)	(0.4%)	(0.2%)	(0.5%)	(3.7%)	(0.3%)
VGG-11	0.3%	0.2%	1.1%	7.0%	1.4%	0.2%
	(0.3%)	(0.2%)	(0.6%)	(1.1%)	(0.2%)	(0.1%)
ConvNeXt-Ti	1.5%	1.2%	1.1%	1.8%	1.5%	0.6%
	(1.0%)	(0.8%)	(0.6%)	(0.4%)	(0.7%)	(0.3%)

Table 10: Average relative contributions (and standard errors) of single blocks to encoding for models fine-tuned with AdamW on CelebA with rare skew

Model	Bl. 0	Bl. 1	Bl. 2	Bl. 3	Bl. 4	Bl. 5
VGG-11	4.1%	2.2%	-3.6%	-6.1%	-56.7%	-1.9%
	(0.9%)	(1.6%)	(2.1%)	(7.6%)	(12.7%)	(0.7%)

Table 11: Average test error rates (and standard errors) on the clean (first and third row) and fully skewed (second and fourth row) CelebA dataset of clean models intervened with sets  $A = [m] \setminus \{i\}$  for VGG-11 architecture fine-tuned with AdamW on common (top) and rare (bottom) skews

Skewed	$\{-0\}$	$\{-1\}$	$\{-2\}$	$\{-3\}$	$\{-4\}$	$\{-5\}$	Clean
21.3%	20.7%	20.8%	20.6%	20.5%	32.5%	22.0%	6.0%
(0.7%)	(0.6%)	(0.6%)	(0.9%)	(0.9%)	(1.9%)	(0.6%)	(0.1%)
0.31%	0.31%	0.31%	0.35%	0.50%	0.49%	0.31%	5.09%
(0.01%)	(0.02%)	(0.02%)	(0.02%)	(0.06%)	(0.05%)	(0.01%)	(0.04%)
11.0%	10.8%	10.9%	11.2%	11.2%	13.7%	11.1%	6.0%
(0.3%)	(0.3%)	(0.4%)	(0.4%)	(0.2%)	(0.7%)	(0.4%)	(0.1%)
0.64%	0.67%	0.66%	0.67%	0.75%	0.56%	0.63%	5.09%
(0.04%)	(0.04%)	(0.05%)	(0.06%)	(0.05%)	(0.01%)	(0.04%)	(0.04%)

## B TRAINING FROM SCRATCH

This section presents the general trends for models trained from scratch observed in our experiments. We didn’t train ConvNeXt-T model from scratch due to computational constraints. Also, note that we did not manage to train the DeiT-Ti architecture on the Waterbirds dataset from scratch. Thus, experiments for this pair are omitted. As previously, we first report the error rates achieved by models on different datasets in Table 12. As we can see, shortcut learning is exacerbated for models trained from scratch. Also, we see that DeiT models have significantly higher error rates on CIFAR-10 because, generally, ViT architectures are more “data hungry” (Zhu et al., 2023). Also, we can see that AdamW achieves better error rates compared to SGD for ViT architectures, while the opposite is true for CNN architectures.

Table 12: Average clean test error rates (and their standard errors in parenthesis) of clean and skewed models trained from scratch with AdamW (top part) and SGD (bottom part) on rare (first and third sub-parts) and common (second and fourth sub-parts) skews

Model	CIFAR-10 (weak)		CIFAR-10 (strong)		Waterbirds		CelebA	
	Clean	Skewed	Clean	Skewed	Clean	Skewed	Clean	Skewed
DeiT-Ti	18.7% (0.2%)	20.8% (0.3%)	18.9% (0.2%)	41.8% (0.4%)	—	—	7.1% (0.1%)	13.3% (0.1%)
ResNet-18	6.7% (0.2%)	19.8% (0.2%)	7.0% (0.1%)	25.6% (0.2%)	7.1% (0.2%)	26.9% (0.5%)	6.3% (0.1%)	11.3% (0.4%)
VGG-11	6.7% (0.1%)	24.2% (0.3%)	7.0% (0.1%)	28.7% (0.3%)	4.9% (0.2%)	25.0% (0.6%)	6.3% (0.1%)	11.2% (0.4%)
DeiT-Ti	18.4% (0.2%)	25.2% (0.6%)	18.7% (0.1%)	63.3% (0.3%)	—	—	7.1% (0.1%)	22.3% (0.3%)
ResNet-18	6.7% (0.2%)	35.1% (0.4%)	7.0% (0.1%)	48.4% (0.3%)	7.1% (0.2%)	36.7% (0.4%)	6.3% (0.1%)	21.4% (0.6%)
VGG-11	6.7% (0.1%)	46.1% (0.5%)	7.0% (0.1%)	57.5% (0.4%)	4.9% (0.2%)	35.2% (0.5%)	6.3% (0.1%)	20.5% (0.3%)
DeiT-Ti	27.5% (0.3%)	28.2% (0.2%)	27.6% (0.2%)	44.1% (0.3%)	—	—	8.7% (0.2%)	12.7% (0.2%)
ResNet-18	5.6% (0.1%)	18.3% (0.1%)	5.9% (0.1%)	24.5% (0.2%)	6.5% (0.2%)	27.3% (0.8%)	6.3% (0.1%)	11.4% (0.2%)
VGG-11	6.4% (0.1%)	23.1% (0.1%)	6.8% (0.2%)	28.6% (0.2%)	4.9% (0.1%)	25.4% (0.5%)	6.3% (0.1%)	11.2% (0.2%)
DeiT-Ti	27.8% (0.3%)	28.7% (0.3%)	27.4% (0.3%)	59.1% (0.3%)	—	—	8.8% (0.2%)	14.9% (0.3%)
ResNet-18	5.6% (0.1%)	32.6% (0.4%)	5.9% (0.1%)	47.9% (0.3%)	6.5% (0.2%)	36.5% (0.4%)	6.3% (0.1%)	22.0% (0.4%)
VGG-11	6.4% (0.1%)	43.8% (0.5%)	6.8% (0.2%)	57.0% (0.5%)	4.9% (0.1%)	35.2% (0.6%)	6.3% (0.1%)	19.9% (0.2%)

**Localization in a Single Block** Table 13 replicates Table 2 for the models trained from scratch. In this experiment, we observed divergence in some intervened VGG-11 models: contributions of the corresponding models are not included in the mean calculation.<sup>5</sup> Generally, we observe trends similar to those previously observed with the fine-tuned models.

**Localization in the Initial Blocks** Table 15 follows Table 6 for the models trained from scratch. Compared to fine-tuned models, the first layer of transformer models starts to play an important role in spurious feature encoding. At the same time, ViT and CNN architectures demonstrate the opposite trends in spurious feature

<sup>5</sup>Similarly to the fine-tuning case, we did not observe divergence in the initial blocks setting. In the single block setting, we observed divergence in 227 out of 2640 models.

Table 13: Average relative contributions (and standard errors) of single blocks to encoding (top) and forgetting (bottom) for models trained from scratch with AdamW on CIFAR-10 (strong) with common skew

Model	Bl. 0	Bl. 1	Bl. 2	Bl. 3	Bl. 4	Bl. 5
DeiT-Ti	24.1% (1.0%)	9.0% (0.6%)	13.7% (0.9%)	14.2% (1.1%)	11.6% (1.1%)	-1.1% (0.8%)
ResNet-18	0.3% (1.1%)	-17.8% (6.3%)	-23.5% (9.1%)	-0.6% (4.7%)	19.3% (2.1%)	0.6% (1.1%)
VGG-11	3.4% (0.7%)	-	-24.2% -	25.9% (2.8%)	16.9% (3.4%)	0.0% (0.6%)
DeiT-Ti	-0.4% (0.2%)	-1.4% (0.5%)	0.7% (0.5%)	0.3% (0.4%)	0.5% (0.4%)	-0.2% (0.4%)
ResNet-18	0.8% (0.3%)	2.7% (0.4%)	21.8% (6.2%)	18.7% (2.2%)	23.3% (2.1%)	-0.1% (0.3%)
VGG-11	0.7% (0.4%)	61.2% (21.7%)	63.7% (28.2%)	57.1% (12.6%)	-	1.4% (0.2%)

encoding. Specifically, for CIFAR-10 and CelebA, ViT architectures tend to encode the spurious feature earlier when trained from scratch compared to fine-tuning, while CNN architectures tend to encode the spurious feature later. However, models trained from scratch seem to encode the background skew in earlier layers compared to the fine-tuned models.

Additionally, all architectures tend to forget the core feature in the latter layers when trained from scratch (however, this trend is less pronounced for ViT architectures). Importantly, the trends about the effects of models on spurious feature encoding also seem to hold for the models trained from scratch. As for the effect of datasets, the watermark skew is still encoded earlier than the sampling skew. However, the background skew is now encoded earlier than the watermark skew.

Table 16 follows Table 3 for the models trained from scratch. Generally, forgetting seems to be even more concentrated in the last and penultimate blocks for models trained from scratch. Also, similarly to the fine-tuned models, common skews seem to induce forgetting in the latter layers. However, it is hard to see more specific trends.

**Main Explanatory Factors** Table 14 follows Table 4 for the models trained from scratch. While the results for the encoding are similar between fine-tuned models and models trained from scratch, the main explanatory factors for the forgetting shift to dataset and model architecture suggesting that forgetting in the models trained from scratch follows different mechanisms compared to fine-tuned models. Dataset and architecture together explain 79.4% and 51.8% of variance in the localization of encoding and forgetting, respectively.

Table 14: Variance explained in relative encoding (left) and forgetting (right) rate by different factors

Encoding				Forgetting			
Dataset	Skew freq.	Model	Optimizer	Dataset	Skew freq.	Model	Optimizer
40.7%	0.4%	23.1%	0.6%	18.8%	4.6%	13.7%	2.1%

Table 15: Average increase rate in relative contributions (and standard errors) of the initial blocks to encoding (top) and forgetting (bottom) for models fine-tuned with AdamW on common skews

Dataset	Model	Bl. 0	Bl. 1	Bl. 2	Bl. 3	Bl. 4	Bl. 5
CIFAR-10 (weak)	DeiT-Ti	75.3% (3.8%)	2.9% (0.9%)	14.2% (2.4%)	6.1% (2.5%)	1.5% (1.6%)	0.2% (0.5%)
	ResNet-18	2.7% (1.3%)	5.4% (0.9%)	14.5% (1.0%)	49.0% (2.0%)	28.6% (0.7%)	0.1% (0.1%)
	VGG-11	1.4% (1.2%)	4.1% (1.0%)	12.0% (1.4%)	36.8% (0.5%)	45.9% (1.0%)	0.0% (0.1%)
	DeiT-Ti	23.7% (1.7%)	18.9% (1.2%)	23.9% (1.5%)	20.6% (1.2%)	13.1% (0.7%)	0.1% (0.1%)
	ResNet-18	0.3% (1.1%)	4.0% (1.0%)	14.1% (1.5%)	48.9% (1.2%)	32.9% (1.1%)	0.1% (0.1%)
	VGG-11	3.4% (0.7%)	-0.5% (1.0%)	13.6% (1.4%)	31.8% (1.3%)	51.9% (0.5%)	0.1% (0.1%)
Waterbirds	ResNet-18	17.2% (1.8%)	7.7% (1.8%)	21.4% (1.0%)	26.5% (1.4%)	26.3% (1.1%)	1.3% (0.6%)
	VGG-11	10.5% (0.8%)	12.1% (1.4%)	33.0% (1.9%)	28.2% (1.1%)	15.6% (0.7%)	0.9% (0.6%)
	DeiT-Ti	20.3% (2.6%)	14.0% (1.8%)	11.1% (2.7%)	13.1% (2.3%)	39.0% (1.9%)	2.8% (0.2%)
	ResNet-18	2.1% (3.7%)	2.4% (1.7%)	6.6% (2.7%)	26.4% (4.5%)	58.5% (5.5%)	4.4% (1.0%)
CelebA	VGG-11	-3.3% (3.7%)	6.5% (2.5%)	5.6% (2.7%)	18.3% (0.9%)	67.0% (1.2%)	6.2% (0.5%)
	DeiT-Ti	1.7% (3.4%)	-11.0% (2.8%)	-2.1% (3.2%)	4.6% (1.5%)	29.3% (4.5%)	77.8% (4.6%)
	ResNet-18	0.6% (0.6%)	0.3% (0.5%)	1.5% (0.6%)	5.1% (0.3%)	15.1% (0.4%)	77.8% (0.2%)
	VGG-11	0.8% (0.3%)	0.5% (0.3%)	3.1% (0.1%)	3.4% (0.3%)	12.7% (0.3%)	79.8% (0.3%)
	DeiT-Ti	-0.6% (0.3%)	0.0% (0.4%)	3.7% (0.6%)	7.3% (1.3%)	15.1% (0.8%)	74.9% (1.0%)
	ResNet-18	0.8% (0.3%)	0.6% (0.4%)	2.3% (0.3%)	5.1% (0.4%)	17.5% (0.6%)	73.9% (0.6%)
CIFAR-10 (strong)	VGG-11	0.7% (0.4%)	1.4% (0.4%)	2.6% (0.2%)	4.3% (0.2%)	16.2% (0.3%)	75.1% (0.3%)
	DeiT-Ti	-	-	-	-	-	-
	ResNet-18	3.3% (0.6%)	1.1% (1.2%)	5.7% (1.2%)	13.2% (1.3%)	11.3% (1.6%)	65.7% (1.3%)
	VGG-11	1.9% (0.6%)	2.4% (0.4%)	5.6% (0.4%)	11.9% (1.3%)	16.1% (1.0%)	62.3% (1.1%)
Waterbirds	ResNet-18	0.5% (0.5%)	2.0% (0.3%)	-0.3% (0.2%)	1.9% (0.3%)	13.0% (1.1%)	83.2% (1.0%)
	VGG-11	0.6% (0.6%)	-0.7% (0.5%)	1.1% (0.4%)	3.2% (0.5%)	6.9% (0.9%)	89.3% (0.7%)
	DeiT-Ti	0.0% (0.4%)	0.4% (0.3%)	1.0% (0.5%)	3.0% (0.4%)	9.8% (0.9%)	86.1% (1.4%)
	ResNet-18	-	-	-	-	-	-
	VGG-11	-	-	-	-	-	-
CelebA	DeiT-Ti	-	-	-	-	-	-
	ResNet-18	-	-	-	-	-	-
	VGG-11	-	-	-	-	-	-
	DeiT-Ti	-	-	-	-	-	-

Table 16: Average increase rate in relative forgetting (and standard errors) of the initial blocks of DeiT-Ti (top) and ResNet-18 (bottom) models trained from scratch on CIFAR-10 (strong)

Frequency	Optimizer	Bl. 0	Bl. 1	Bl. 2	Bl. 3	Bl. 4	Bl. 5
Rare	AdamW	-1.4%	-1.5%	4.2%	9.4%	18.3%	71.3%
		(1.4%)	(1.1%)	(0.9%)	(1.6%)	(1.1%)	(1.6%)
	SGD	-8.8%	-1.5%	1.0%	5.4%	26.7%	77.4%
		(1.5%)	(1.6%)	(1.0%)	(0.7%)	(0.5%)	(1.4%)
Common	AdamW	-0.6%	0.0%	3.7%	7.3%	15.1%	74.9%
		(0.3%)	(0.4%)	(0.6%)	(1.3%)	(0.8%)	(1.0%)
	SGD	-4.7%	-1.7%	0.6%	3.6%	19.0%	83.6%
		(1.1%)	(0.8%)	(0.3%)	(0.5%)	(0.8%)	(1.2%)
Rare	AdamW	1.1%	0.8%	3.7%	7.1%	20.7%	66.8%
		(0.8%)	(0.8%)	(0.4%)	(0.4%)	(0.6%)	(0.5%)
	SGD	1.9%	1.4%	4.4%	6.6%	26.9%	59.2%
		(0.8%)	(0.7%)	(0.6%)	(0.5%)	(0.5%)	(0.5%)
Common	AdamW	0.8%	0.6%	2.3%	5.1%	17.5%	73.9%
		(0.3%)	(0.4%)	(0.3%)	(0.4%)	(0.6%)	(0.6%)
	SGD	0.8%	1.2%	2.5%	4.5%	21.4%	70.0%
		(0.2%)	(0.2%)	(0.2%)	(0.2%)	(0.5%)	(0.4%)

## C DETAILS OF TRAINING

We use the standard AdamW and SGD (with Nesterov momentum) optimizers from PyTorch and cosine learning scheduler with linear warm-up. Table 17 reports the number of training epochs. The hyper-parameters of optimizers are listed in Table 18 (for fine-tuning) and Table 19 (for training from scratch). For training, we use standard augmentations: random resized crop and random horizontal flip. For CelebA and Waterbirds, we use the same augmentation parameters as Sagawa\* et al. (2020). For CIFAR, we use scale (0.8, 1.0) and ratio (3/4, 4/3). We resize all images to size  $224 \times 224$  for both training and evaluation. For ResNet-18, VGG-11, and ConvNeXt-T fine-tuning, we used the default weights from the TorchVision (TorchVision maintainers and contributors, 2016) library. For DeiT-Ti fine-tuning, we used the default weights from the timm (Wightman, 2019) library.

We use the standard `train` CIFAR-10 and CUB-200-2011 (Wah et al., 2011) splits for the training on CIFAR-10 and Waterbirds. We use the union of `train` and `validation` splits for the training on CelebA. We use `test` splits of the considered datasets for the evaluation. To make an MNIST watermark, we use `train` split for training data and `test` split for the evaluation data. We use non-overlapping data from `train` split of the Places365 (Zhou et al., 2017) dataset as backgrounds for the Waterbirds dataset, following Sagawa\* et al. (2020).

ResNet, VGG, and DeiT were fine-tuned on cloud nodes with 4 A100 GPUs. ConvNeXt was fine-tuned on cloud nodes with 2 H200 GPUs. For CIFAR and CelebA, models were trained from scratch on local cluster nodes with 2 H200 GPUs. Finally, for Waterbirds, ResNet-18 models were trained on cloud nodes with 4 L4 GPUs, and VGG-11 models were trained on cloud nodes with 4 A100 GPUs. Fine-tuning experiments took around 590 A100-hours and 200 H200-hour. Training from scratch experiments took around 1245 H200-hours, 765 A100-hours, and 960 L4-hours together.

Table 17: Number of training epochs

Fine-tuning			Training from scratch		
CIFAR-10	Waterbirds	CelebA	CIFAR-10	Waterbirds	CelebA
20	20	2	100	1000	10

Table 18: Hyperparameters for fine-tuning

Optimizer	Model	Parameter	Value
AdamW	DeiT-Ti	<code>batch_size</code>	256
		<code>lr</code>	$1e-5 \times \text{batch\_size}^{0.5}$
		<code>weight_decay</code>	0.01
		<code>min_lr</code>	$1e-7 \times \text{batch\_size}^{0.5}$
		Share of warm-up steps	2%
	ResNet-18	<code>batch_size</code>	256
		<code>lr</code>	$1e-5 \times \text{batch\_size}^{0.5}$
		<code>weight_decay</code>	0.01
		<code>min_lr</code>	$1e-7 \times \text{batch\_size}^{0.5}$
		Share of warm-up steps	2%
	VGG-11	<code>batch_size</code>	256
		<code>lr</code>	$1e-5 \times \text{batch\_size}^{0.5}$
		<code>weight_decay</code>	0.01
		<code>min_lr</code>	$1e-7 \times \text{batch\_size}^{0.5}$
		Share of warm-up steps	2%
	ConvNeXt-T	<code>batch_size</code>	256
		<code>lr</code>	$1e-5 \times \text{batch\_size}^{0.5}$
		<code>weight_decay</code>	0.01
		<code>min_lr</code>	$1e-7 \times \text{batch\_size}^{0.5}$
		Share of warm-up steps	2%
	SGD	<code>batch_size</code>	256
		<code>lr</code>	$2e-5 \times \text{batch\_size}$
		<code>weight_decay</code>	0.0001
		<code>momentum</code>	0.9
		<code>min_lr</code>	$5e-7 \times \text{batch\_size}$
		Share of warm-up steps	2%
		<code>batch_size</code>	256
		<code>lr</code>	$1e-4 \times \text{batch\_size}$
		<code>weight_decay</code>	0.0001
		<code>momentum</code>	0.9
	ResNet-18	<code>min_lr</code>	$5e-7 \times \text{batch\_size}$
		Share of warm-up steps	2%
		<code>batch_size</code>	256
		<code>lr</code>	$1e-4 \times \text{batch\_size}$
		<code>weight_decay</code>	0.0001
	VGG-11	<code>momentum</code>	0.9
		<code>min_lr</code>	$5e-7 \times \text{batch\_size}$
		Share of warm-up steps	2%
		<code>batch_size</code>	256
		<code>lr</code>	$1e-5 \times \text{batch\_size}$
	ConvNeXt-T	<code>weight_decay</code>	0.0001
		<code>momentum</code>	0.9
		<code>min_lr</code>	$5e-7 \times \text{batch\_size}$
		Share of warm-up steps	2%

Table 19: Hyperparameters for training from scratch

Optimizer	Model	Parameter	Value
AdamW	DeiT-Ti	<code>batch_size</code>	256
		<code>lr</code>	$5e-5 \times \text{batch\_size}^{0.5}$
		<code>weight_decay</code>	0.01
		<code>min_lr</code>	$1e-7 \times \text{batch\_size}^{0.5}$
		Share of warm-up steps	5%
ResNet-18		<code>batch_size</code>	256
		<code>lr</code>	$5e-3 \times \text{batch\_size}^{0.5}$
		<code>weight_decay</code>	0.01
		<code>min_lr</code>	$5e-5 \times \text{batch\_size}^{0.5}$
		Share of warm-up steps	5%
VGG-18		<code>batch_size</code>	256
		<code>lr</code>	$5e-3 \times \text{batch\_size}^{0.5}$
		<code>weight_decay</code>	0.01
		<code>min_lr</code>	$5e-5 \times \text{batch\_size}^{0.5}$
		Share of warm-up steps	5%
SGD	DeiT-Ti	<code>batch_size</code>	256
		<code>lr</code>	$2e-4 \times \text{batch\_size}$
		<code>weight_decay</code>	0.0001
		<code>momentum</code>	0.9
		<code>min_lr</code>	$5e-7 \times \text{batch\_size}$
ResNet-18		Share of warm-up steps	5%
		<code>batch_size</code>	256
		<code>lr</code>	$5e-3 \times \text{batch\_size}$
		<code>weight_decay</code>	0.0001
		<code>momentum</code>	0.9
VGG-18		<code>min_lr</code>	$2e-5 \times \text{batch\_size}$
		Share of warm-up steps	5%
		<code>batch_size</code>	256
		<code>lr</code>	$5e-3 \times \text{batch\_size}$
		<code>weight_decay</code>	0.0001
		<code>momentum</code>	0.9
		<code>min_lr</code>	$2e-5 \times \text{batch\_size}$
		Share of warm-up steps	5%

## D MISCELLANEOUS

### D.1 Licenses of the Used Assets

**Datasets** To the authors' best knowledge, the used datasets have the following licenses (see Table 20).

Table 20: Licenses of the used datasets

Dataset	License (or known restrictions)
MNIST (Lecun et al., 1998)	CC BY-SA 3.0
CIFAR-10 (Krizhevsky, 2009)	no license specified
CUB-200-2011 (Wah et al., 2011)	non-commercial research and educational restriction
Places365 (Zhou et al., 2017)	academic and educational restriction
CelebA (Liu et al., 2015)	Custom non-commercial research license

**Pre-Trained Weights** To the authors' best knowledge, the used pre-trained models have the following licenses (see Table 21).

Table 21: Licenses of the used pre-trained models

Model	License (or known restrictions)
ResNet-18	BSD-3 (from the TorchVision library) and non-commercial use (from ImageNet)
VGG-11	BSD-3 (from the TorchVision library) and non-commercial use (from ImageNet)
DeiT-Ti	Apache 2.0 (from the original paper) and non-commercial use (from ImageNet)